Direct and indirect probes of Goldstone dark matter

Tommi Alanne,[1,*] Matti Heikinheimo,[2,3,†] Venus Keus,[2,3,‡] Niko Koivunen,[2,3,§] and Kimmo Tuominen[2,3,¶]

[1]*Max-Planck-Institut für Kernphysik, Saupfercheckweg 1, 69117 Heidelberg, Germany*
[2]*Department of Physics, University of Helsinki, P.O. Box 64, FI-00014 Helsinki, Finland*
[3]*Helsinki Institute of Physics, University of Helsinki, P.O. Box 64, FI-00014 Helsinki, Finland*

(Received 19 December 2018; published 24 April 2019)

There exists a general model framework where dark matter can be a vanilla weakly-interacting-massive-particle-like thermal relic with a mass of $\mathcal{O}(100\ \mathrm{GeV})$, but it still escapes direct detection. This happens if the dark matter particle is a Goldstone boson whose scattering with ordinary matter is suppressed at low energy due to momentum-dependent interactions. We outline general features of this type of models and analyze a simple realization of these dynamics as a concrete example. In particular, we show that although direct detection of this type of dark matter candidate is very challenging, the indirect detection can already provide relevant constraints. Future projections of the indirect-detection experiments allow for even more stringent exclusion limits and can rule out models of this type.

DOI: 10.1103/PhysRevD.99.075028

I. INTRODUCTION

Over recent years the paradigm of dark matter (DM) as a thermal relic has been heavily challenged by the results from direct-detection experiments, which systematically provide more stringent bounds on the strength of the interaction between dark and ordinary matter [1–3]. One possible interpretation of these results is that DM constitutes a secluded sector that is very feebly coupled with the Standard Model (SM). In this type of freeze-in models [4–6] the portal coupling of $\mathcal{O}(10^{-10})$ allows the observed DM abundance to be produced out of equilibrium without ever equilibrating with the SM heat bath. Consequently, models of this type are usually completely invisible in the direct-detection experiments.

However, several solutions to address this issue also within the standard thermal-relic paradigm have been proposed. For example, a large enough particle content beyond the SM could make the cross sections probed in direct-detection experiments distinct from the cross sections affecting the freeze-out dynamics in the early universe [7]. Such nonminimal hidden-sector models, on the other hand, generally extend the usual problems of explaining the origins and hierarchies of the required mass scales and couplings.

It would therefore be worthwhile to outline general features of models where similar effects could be achieved with minimal particle content. In this paper, we investigate simple scalar extensions of the SM where the DM arises as a pseudo-Goldstone boson of an approximate global symmetry; examples of such models have been studied recently in, e.g., [8–15]. Since generally the interactions of Goldstone bosons are momentum suppressed, this will naturally suppress the DM-nucleon elastic scattering cross section relevant for direct search experiments, which operate in the limit of zero-momentum transfer. On the other hand, the annihilation cross section of pseudo-Goldstone bosons does not vanish in the nonrelativistic limit, as the momentum transfer in this process contains a nonzero contribution from the rest mass of the annihilating particles. Therefore, in this class of models, DM with the observed abundance can be produced as a thermal relic, while the direct-detection cross section is small enough for the DM to have escaped all present direct searches.

The indirect DM searches, on the other hand, probe the same annihilation process that is relevant for determining the DM abundance. Since this scattering amplitude does not vanish in the limit of zero incoming three-momentum, the indirect-detection signal expected from a pseudo-Goldstone DM particle is of a similar magnitude as that of a generic weakly-interacting-massive-particle (WIMP). Indeed, indirect-detection limits turn out to be very constraining for such DM candidates, and future prospects for observing pseudo-Goldstone DM up to a couple hundred GeV masses in indirect searches are promising.

There is, however, a caveat to the above simple picture: to account for a finite mass of the Goldstone boson DM

*tommi.alanne@mpi-hd.mpg.de
†matti.heikinheimo@helsinki.fi
‡venus.keus@helsinki.fi
§niko.koivunen@helsinki.fi
¶kimmo.i.tuominen@helsinki.fi

candidate, an explicit breaking of the global symmetry is required. Since the vanishing of the direct-detection cross section at zero-momentum transfer rests on the foundation of the underlying global symmetry and the resulting Goldstone nature of the DM particle, it should not be expected to strictly hold in the presence of explicit symmetry breaking. This issue has been investigated in recent works [12–14], where one-loop contributions to the direct-detection amplitude were considered. It turns out indeed that the one-loop contribution does not vanish in the zero-momentum transfer limit, and the resulting prediction for the direct-detection event rate is considerably larger than the tree-level prediction. However, for most parts of the parameter space, the pseudo-Goldstone DM still remains concealed below the neutrino floor and thus hidden from direct detection.

To demonstrate these mechanisms and effects quantitatively, we will use an effective model with the $O(N)/O(N-1)$ symmetry-breaking pattern as an example. However, our analysis can be applied to all models where the hidden-sector degrees of freedom (d.o.f.) consist of Goldstone bosons and one massive scalar mixing with the Higgs boson. We will discuss how the effective theory with the leading symmetry-breaking operators of dimensions two and four may emerge from simple high-energy dynamics, thus approaching the issue of accounting for the effects of explicit symmetry breaking from a top-down direction, and compare the results to the bottom-up approach of computing the radiative corrections in the low-energy effective theory [10,12–14]. We will present a compilation of current experimental constraints from direct and indirect observations on DM scattering as well as from collider experiments.

The paper is organized as follows: In Sec. II we will outline the general model framework and relevant constraints. Then, in Sec. III we will carry out a detailed quantitative analysis for single component Goldstone DM and show how various experimental and observational constraints operate. In Sec. IV we will present our conclusions and outlook for further work. Some analytic results relevant for the analysis and the nonlinear representation of the model are collected in the Appendixes.

II. GENERAL MODEL FRAMEWORK AND CONSTRAINTS

We consider a scenario where DM arises as a pseudo-Goldstone boson associated with the breaking of an approximate global symmetry. Such a DM candidate emerges naturally, for example, in models featuring new strong dynamics leading to a spectrum of mesons at low energies (see, e.g., Refs. [16–19]). To keep the discussion simple, and to establish generic features of this type of DM, we will here treat the effective theory d.o.f. as elementary fields.

Concretely, we consider extending the SM with a scalar field, S, transforming under some irreducible N-dimensional representation of a global symmetry G. The scalar field is assumed to develop a vacuum expectation value (VEV), $\langle S\rangle = w$, such that the symmetry breaks to a subgroup G'. We consider explicitly a class of models with the symmetry-breaking pattern $O(N)/O(N-1)$. Then the relevant low-energy d.o.f. are parametrized in terms of an $O(N)$ vector

$$\Sigma = (\eta_1, \eta_2, \ldots, \eta_{N-1}, \sigma), \tag{1}$$

where σ is the field direction along which the VEV of Σ develops. Then, the effective Lagrangian for the singlet sector and its interactions with the visible sector is

$$\mathcal{L} = \frac{1}{2}\partial_\mu\sigma\partial^\mu\sigma + \frac{1}{2}\partial\eta_a\partial\eta_a - V(\Sigma, H), \tag{2}$$

where H is the usual SM Higgs field. The potential $V(\Sigma, H)$ is given by

$$V(\Sigma, H) = \mu_H^2 H^\dagger H + \frac{1}{2}\mu_\Sigma^2\Sigma^\dagger\Sigma + \lambda_H(H^\dagger H)^2 + \frac{\lambda_{H\Sigma}}{2}(H^\dagger H)\Sigma^\dagger\Sigma + \frac{\lambda_\Sigma}{4}(\Sigma^\dagger\Sigma)^2 + V_{\rm sb}, \tag{3}$$

where $\Sigma^\dagger\Sigma = \sigma^2 + \eta_a\eta_a$ preserves the O(N) symmetry and $V_{\rm sb}$ contains the contributions containing the symmetry-breaking linear combination $\sigma^2 - \eta_a\eta_a$.

The field η^a will be a DM candidate as it is protected against decay by a symmetry within G'. Of course, to constitute cold a DM of thermal origin, it must be massive and the symmetry G must be explicitly broken. On the effective Lagrangian level, one could include the leading symmetry-breaking term $M_\eta^2\eta_a\eta_a$, which would arise from some higher scale physics coupling with Σ and integrated out to obtain the low-energy effective theory, Eq. (2). A simple possibility would be a heavy fermion Ψ coupling with all components η^a via

$$\Delta\mathcal{L}_{\rm UV} \supset i g_P \eta^a \bar{\Psi}\gamma_5\Psi. \tag{4}$$

When integrated out, this heavy fermion yields a nonzero mass for all Goldstone bosons, $M_\eta^2 \sim g_P^2 M_\psi^2$. Furthermore, contributions to four point couplings between components Σ^a are generated, but these are parametrically smaller, of order $\sim g_P^4$.

Taking into account the coupling with the Higgs would lead to further explicit symmetry-breaking terms of the form $\lambda_X H^\dagger H(\sigma^2 - \eta_a\eta_a)$, where $\lambda_X \sim \lambda_{H\Sigma} g_P^4$. We will therefore take

$$V_{\rm sb} = -\frac{1}{2}\mu_X^2(\sigma^2 - \eta_a\eta_a) - \frac{\lambda_X}{2}(H^\dagger H)(\sigma^2 - \eta_a\eta_a). \tag{5}$$

With these definitions, we can now see how the essential dynamics for DM scattering on ordinary matter can be

inferred from the Lagrangian, Eq. (2). As Σ and H obtain their VEVs, $\langle\Sigma\rangle = w$ and $\langle H\rangle = v$, the effective potential in Eq. (3) is minimized by requiring

$$\mu_H^2 = -\frac{1}{2}(2\lambda_H v^2 + (\lambda_{H\Sigma} - \lambda_X)w^2),$$
$$\mu_\Sigma^2 = -\frac{1}{2}(2\lambda_\Sigma w^2 + (\lambda_{H\Sigma} - \lambda_X)v^2 - 2\mu_X^2). \quad (6)$$

The scalar field σ will mix with the neutral component the doublet H; the mass eigenstates are the physical Higgs boson, h^0, and another massive scalar, H^0. These mass eigenstates are given by

$$\begin{pmatrix} h^0 \\ H^0 \end{pmatrix} = \begin{pmatrix} \cos\alpha & -\sin\alpha \\ \sin\alpha & \cos\alpha \end{pmatrix}\begin{pmatrix} \phi \\ \sigma \end{pmatrix}, \quad (7)$$

with

$$\tan(2\alpha) = -\frac{(\lambda_{H\Sigma} - \lambda_X)vw}{\lambda_H v^2 - \lambda_\Sigma w^2}. \quad (8)$$

Now we can solve λ_Σ from Eq. (8) and trade λ_H, w, and μ_X^2 for the masses of the eigenstates, m_{h^0}, m_{H^0}, m_η. Identifying the lightest eigenstate with the SM Higgs, $m_{h^0} = 125$ GeV, leaves us with $\lambda_{H\Sigma}$, m_{H^0}, m_η, α, and λ_X as input parameters.

The interactions between SM matter and DM arise from the SM Yukawa couplings providing the usual link between the Higgs doublet and ordinary matter, and from the coupling of the DM with both the Higgs and the singlet scalar, σ. Because of the mixing of the scalar, the scattering of DM on ordinary matter is mediated by both scalar mass eigenstates, h^0 and H^0.

Generally, the scattering of Goldstone bosons is proportional to the momentum transfer in the process, and one expects that the DM scattering cross section on ordinary matter becomes suppressed. In the model setup described above, neglecting λ_X, which we have argued to be suppressed, one finds that

$$\frac{d\sigma_{SI}}{d\cos\theta} \sim \frac{\lambda_{HS}^2 f_N^2 m_N^2}{(m_{h^0}^2 - t)^2(m_{H^0}^2 - t)^2}t^2. \quad (9)$$

The direct-detection cross section vanishes as $t \to 0$.

However, there is an important refinement of this argument: the effects of the symmetry-breaking contributions we have introduced above are $\mathcal{O}(t^0)$ rather than vanishing proportionally to the momentum transfer. As a result, the symmetry-breaking contributions can quantitatively be significant, even if generated at one-loop or higher order, and must be treated with care. We study this in detail in Sec. III, where we will also quantify the effects arising from the nonzero values of the coupling λ_X.

Let us then consider the general features of the constraints from collider searches and cosmological and astrophysical observations that pertain to the pseudo-Goldstone DM model. First, the observed abundance of DM must be produced as a thermal relic. This implies that the thermal annihilation cross section must satisfy $\langle\sigma v_{rel}\rangle_0 \simeq 3 \times 10^{-26}$ cm$^3/s$. We focus on a scenario where the DM is the lightest non-SM particle and consider the annihilation cross section to SM final states.

Second, models with a hidden-sector coupling to the visible sector via a scalar portal are constrained by collider experiments in two respects: The mass eigenstates are mixtures of the neutral component of the SU(2) scalar doublet and the singlet scalar. The associated mixing angle, α, is constrained from the Higgs couplings measurements by $\sin\alpha \lesssim 0.3$ [20]. Additionally, if the hidden sector contains states that are lighter than half of the mass of the Higgs boson, they will contribute to the invisible Higgs decays. Such decays are currently bounded by $\mathrm{Br}(h^0 \to \mathrm{inv}) \leq 0.23$ [21,22].

Third, direct-detection experiments provide stringent exclusion bounds for a vanilla scalar DM with a mass of $\mathcal{O}(100$ GeV). However, in the framework studied here, the Goldstone nature of the DM particle relaxes the direct-detection bounds due to the momentum suppression of the cross section, as discussed above. Generally, in this scenario the WIMP couples to the nucleus via the Higgs boson, h^0, and the heavier mass eigenstate, H^0. The strength of the interaction depends on the mixing pattern of the scalars and whether the WIMP is a scalar or a fermion. In both cases, the Higgs-nucleon coupling is of the form $f_N m_N/v$, with $m_N = 0.946$ GeV, where we neglect the small differences between neutrons and protons. The effective Higgs-nucleon coupling,

$$f_N \equiv \frac{1}{m_N}\sum_q \langle N|m_q\bar{q}q|N\rangle, \quad (10)$$

describes the normalized total quark-scalar current within the nucleon. The quark currents of the nucleon have been the subject of intensive lattice studies, supplemented by chiral perturbation theory methods and pion nucleon scattering analysis. Consequently, the current value for $f_N \simeq 0.3$ [23–25] is fairly well determined. The spin-independent cross section for a WIMP scattering on nuclei is computed by considering the t-channel exchange of h^0 and H^0. Because of the Goldstone nature of the DM candidate, even in the presence of the symmetry-breaking operators, this cross section is suppressed, allowing for the compatibility with the current direct search limits. We will show this in detail for an explicit model in the next section.

Finally, the model is constrained by indirect detection. The indirect-detection experiments attempt to observe the annihilation products of DM particles originating from regions of high DM number density in the cosmos, such as the central regions of DM halos. The nonobservation of such signals leads to an upper limit on the DM annihilation

cross section. Currently the most constraining limits for our mass range of interest are from Fermi-LAT observations of dwarf spheroidal satellite galaxies of the Milky Way [26]. While the direct-detection cross section is strongly suppressed at low momentum transfer for Goldstone DM, this is not generally true for the annihilation cross section. Indeed, in the simplest Goldstone-DM models, the annihilation amplitude is an s wave, so that a nonzero amplitude at zero incoming three-momentum exists, making indirect detection a promising avenue for observing Goldstone DM.

We will quantify all the above constraints in the next section for an explicit model of Goldstone DM.

III. A MODEL EXAMPLE

We will now consider the model introduced in Sec. II in the simplest case of O(2) symmetry. This scenario is equivalent to the extension of the SM with a complex singlet featuring a global U(1) symmetry [27]. Then the DM candidate is a single Goldstone boson. Theories where Goldstone DM forms a degenerate multiplet can easily be addressed using our results together with simple scaling: the event rate in direct-detection experiments scales linearly with the degeneracy, g, while the rate in indirect detection is independent of g.

For most of the analysis, we set symmetry-breaking coefficient λ_X in Eq. (5) to zero and focus on the effect of the leading symmetry-breaking term, $\mu_X^2 \neq 0$. We also show the quantitative effect from $\lambda_X \neq 0$ on our results.

A. Relic abundance

To determine the relic abundance of the scalar η, we compute the total annihilation cross section into SM particles and compare it with the standard thermal annihilation cross section, $\langle \sigma v_{\rm rel} \rangle_0 \simeq 3 \times 10^{-26}\ {\rm cm}^3/{\rm s}$, as described in Sec. II. The following annihilation channels need to be taken into account: $\eta\eta \to h^0 h^0$, VV, and $\bar{f}f$, where V denotes the electroweak gauge bosons, $V = W, Z$, and f are the SM fermions.[1] The annihilation cross sections to these three distinct final states are given in Appendix A. Following Ref. [28], we include the four-body final states due to the virtual W and Z exchange using the full width of the Higgs [29] in the calculation of the annihilation cross section in the mass range $m_{h^0}/2 \leq m_\eta \leq 100$ GeV. We show the curve where $\langle \sigma v_{\rm rel} \rangle = \langle \sigma v_{\rm rel} \rangle_0$ for $m_{H^0} = 500$, 750 GeV, $\alpha = 0.3$, $\lambda_X = 0$ in Figs. 1 and 2 along with the constraints from invisible Higgs decays and direct-detection searches, and in Fig. 4 together with the indirect-detection bounds.

[1]We are interested in the case where η is a Goldstone boson and thus lighter than H^0. Therefore, we do not consider $\eta\eta \to h^0 H^0$, $H^0 H^0$ channels.

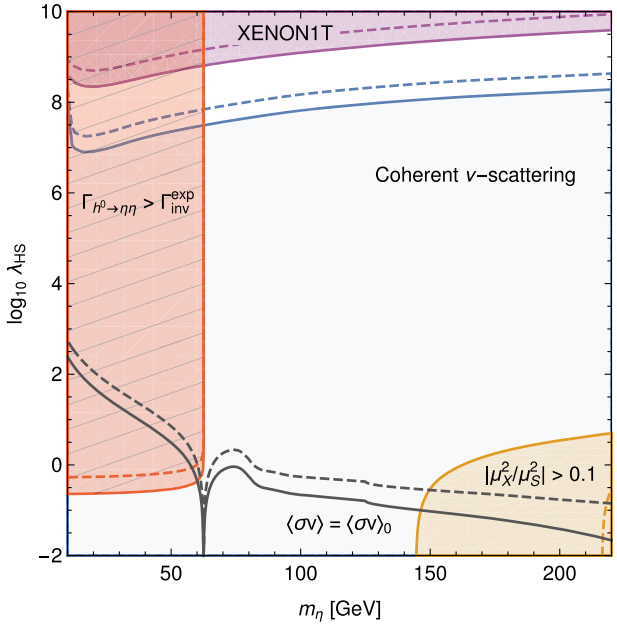

FIG. 1. The current limits from XENON1T on the spin-independent scattering cross section of DM off of nuclei assuming the tree-level momentum-suppressed estimate of the cross sections (upper purple shaded region) and invisible Higgs decays (red shaded region on left), and the region where the SI cross section reaches the coherent neutrino scattering cross section (lower blue region). The limits are for $m_{H^0} = 500\,{\rm GeV}$ and $\alpha = 0.3$. The dashed curves show the change for $m_{H^0} = 750$ GeV. The yellow shaded region shows where $\mu_X^2/\mu_S^2 > 0.1$. The gray solid (dashed) curve shows where the observed DM abundance is achieved for $m_{H^0} = 500$ GeV (750 GeV).

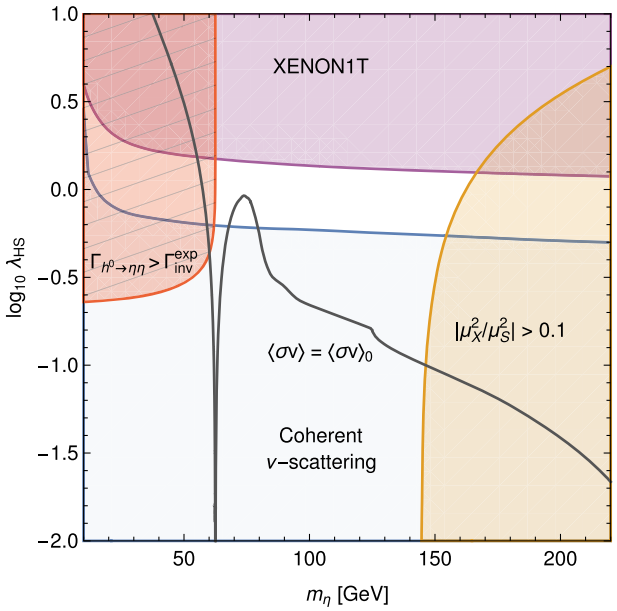

FIG. 2. The corresponding plot to Fig. 1, with the dominant one-loop contributions taken into account, for the DM-nucleon cross section (see the text for details). We plot here only the $m_{H^0} = 500$ GeV curves for clarity.

B. Invisible Higgs decays

If $m_\eta < m_{h^0}/2$, one needs to take into account the constraints from invisible Higgs decays, currently bound to be $\mathrm{Br}(h^0 \to \mathrm{inv}) \leq 0.23$ [21,22]. The Higgs total decay width to the visible SM channels is $\Gamma_{h^0} = 4.07$ MeV for $m_{h^0} = 125$ GeV [30], and the $h^0 \to \eta\eta$ width is given by

$$\Gamma_{h^0\to\eta\eta} = \frac{\lambda^2_{h^0\eta\eta}}{32\pi m_{h^0}}\sqrt{1-\frac{4m_\eta^2}{m_{h^0}^2}}, \tag{11}$$

where

$$\lambda_{h^0\eta\eta} = \frac{(\lambda_{HS}-\lambda_X)m_{h^0}^2 v}{\cos\alpha(m_{h^0}^2 - m_{H^0}^2)} + 2\lambda_X v\cos\alpha. \tag{12}$$

We show the excluded region as a function of DM mass and λ_{HS} for $m_{H^0} = 500$, 750 GeV, $\alpha = 0.3$, $\lambda_X = 0$ superimposed with direct-detection bounds in Figs. 1 and 2. The invisible Higgs decays exclude the full parameter space for a light DM except for the very narrow resonance region where $m_\eta \approx m_{h^0}/2$.

C. Direct detection

1. Tree-level estimate

At tree level, the spin-independent (SI) direct-detection cross section is

$$\frac{\mathrm{d}\sigma_{\mathrm{SI}}}{\mathrm{d}\cos\theta} = \frac{\lambda^2_{\mathrm{eff}} f_N^2 m_N^2 \mu_R^2}{8\pi m_\eta^2}, \tag{13}$$

where $\mu_R = m_N m_\eta/(m_N + m_\eta)$ is the reduced mass of the η-nucleon system, and

$$\lambda_{\mathrm{eff}} = \frac{\lambda_{HS} t}{(m_{h^0}^2 - t)(m_{H^0}^2 - t)} - \frac{2\lambda_X[\sin^2\alpha(m_{h^0}^2 - t/2) + \cos^2\alpha(m_{H^0}^2 - t/2)]}{(m_{h^0}^2 - t)(m_{H^0}^2 - t)}. \tag{14}$$

Note that the first term vanishes at zero-momentum transfer, as expected for a Goldstone boson. Furthermore, note that this result persists in the presence of the soft symmetry-breaking mass term for η; the nonzero contributions at zero-momentum transfer arise only due to the explicit symmetry-breaking term, λ_X, in the scalar potential in Eq. (3).

We show in Fig. 1 the current limit from XENON1T experiment [3], along with the tentative boundary of the coherent neutrino-scattering cross section [31] and the experimental bound for invisible Higgs decays [21,22] in the (m_η, λ_{HS}) plane in the case of $\lambda_X = 0$ for fixed values of $m_{H^0} = 500$ GeV and $\alpha = 0.3$. For higher values of m_{H^0}, the boundaries move upwards in the plane; lowering α has the same effect on the invisible-Higgs-decay boundary. The dashed curves show the case of $m_{H^0} = 750$ GeV. We have chosen a constant incoming velocity of the DM particles,[2] $v_\eta = 10^{-3}c$. The gray solid (dashed) curve shows where the observed DM abundance is obtained for $m_{H^0} = 500$ GeV (750 GeV); the whole curve lies beneath the neutrino floor. Note that the highly nonperturbative values of λ_{HS} in Fig. 1 are shown for illustration only. The allowed region of the perturbatively computed relic density curve lies in the domain where the use of perturbation theory is justified. The yellow shaded region in the lower right corner shows where the explicit-breaking mass term, μ_X^2, starts to be sizable in comparison to the symmetry-preserving one, μ_S^2. In Fig. 1 we show $\mu_X^2/\mu_S^2 = 0.1$ as a limit for significant symmetry breaking.

2. One-loop contributions

The soft breaking of the global symmetry by μ_X^2 does not affect the tree-level estimate of the DM-nucleon scattering cross section, and the cross section remains momentum suppressed even in the presence of explicit breaking of the symmetry. Therefore, one expects the quantum corrections to induce contributions that scale as the DM mass, m_η, rather than the momentum transfer, t, to the cross section manifesting the explicit breaking and the pseudo-Goldstone nature of the DM candidate. This, indeed, turns out to be the case, and the one-loop contribution to the DM-nucleon scattering has a piece independent of the momentum transfer that vanishes in the limit of $m_\eta \to 0$. This contribution dominates the DM-nucleon scattering by several orders of magnitude and was estimated in Ref. [10] to be

$$\sigma_{\mathrm{SI}}^{1-\mathrm{loop}} \approx \frac{\sin^2\alpha}{64\pi^5}\frac{m_N^4 f_N^2}{m_{h^0}^4 v^2}\frac{m_{H^0}^2 m_\eta^2}{w^6}, \tag{15}$$

for $m_\eta < m_{H^0}$. The first exact one-loop computations [12,13] point to the same ballpark region, indicating that Eq. (15) only slightly overestimates the cross section. For the purpose of our analysis, we use the conservative estimate of Eq. (15), noting that an order-of-magnitude decrease in the cross section does not alter the qualitative picture.

We show the corresponding plot to Fig. 1, with the dominant one-loop contribution taken into account, in Fig. 2. We only show the $m_{H^0} = 500$ GeV curves for simplicity and refer to Fig. 1 for the change due to increasing the heavy-scalar mass. The other parameter values are as in Fig. 1.

3. Explicit breaking beyond mass terms

In the presence of the quartic explicit-breaking coupling, λ_X, already the tree-level DM-nucleon scattering cross section is sensitive to the breaking and has a piece that

[2]We have checked for a sample of parameter points that integrating over the DM velocity distribution given by the standard halo model gives similar results.

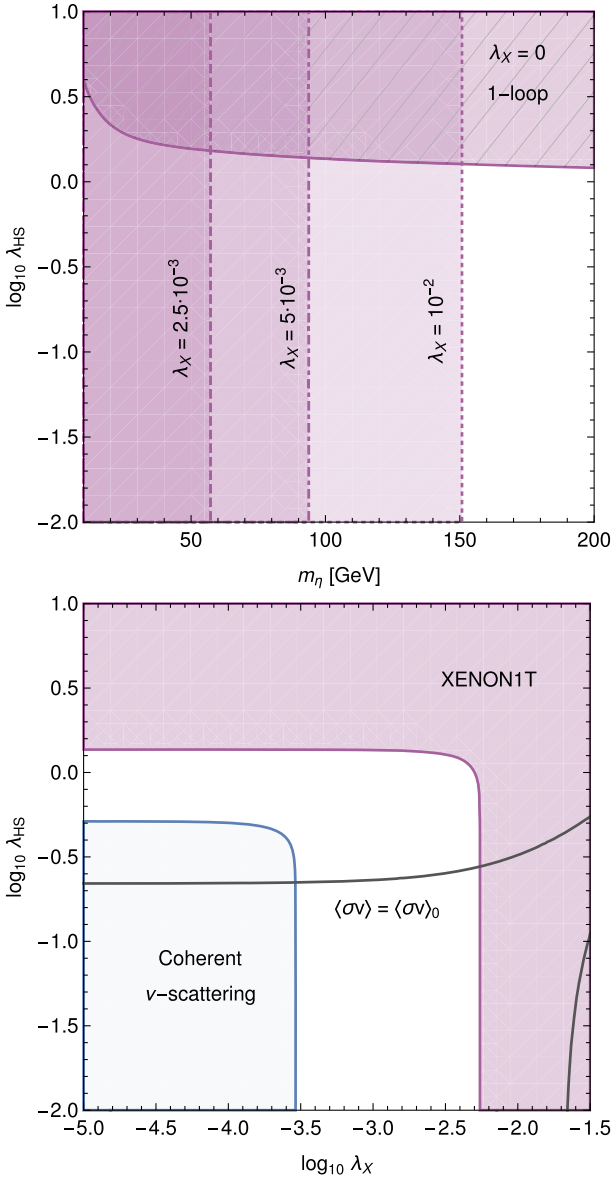

FIG. 3. Top panel: the current limits from XENON1T on the spin-independent scattering cross section of DM off of nuclei for nonzero values of λ_X. Bottom panel: the limits from XENON1T and the neutrino floor in the $(\lambda_X, \lambda_{HS})$ plane for a fixed DM mass of $m_\eta = 100$ GeV and $\alpha = 0.3$. The gray curve shows where the observed DM abundance is obtained.

does not vanish at zero-momentum transfer: the second term in Eq. (14).

In the top panel of Fig. 3, we show how the XENON1T limit changes if the explicit-breaking parameter, λ_X, is turned on; we plot the exclusion regions for fixed values of $\lambda_X = 0$, 2.5×10^{-3}, 5×10^{-3}, 10^{-2}. The bottom panel of Fig. 3 shows the XENON1T exclusion and the neutrino floor along with the curve $\langle\sigma v_{\rm rel}\rangle = \langle\sigma v_{\rm rel}\rangle_0$ in the $(\lambda_X, \lambda_{HS})$ plane for fixed values of $m_\eta = 100$ GeV and $\alpha = 0.3$. Changing α has little effect on the SI cross section, and thus varying α does not noticeably change the plots. These figures show the current direct-detection bounds can be evaded even if the symmetry is only approximate or accidental; for example, for $m_\eta \sim 150$ GeV non-negligible couplings of $\lambda_X \lesssim 0.01$ are still allowed.

D. Indirect detection

The indirect-detection constraints arise from the annihilation of DM particles. The relevant cross section formulas are given in Appendix A. To clarify the discussion, we show here just the annihilation cross section to the $\bar{b}b$ channel in the limit of $\lambda_X = 0$:

$$v_{\rm rel}\cdot\sigma_{\eta\eta\to\bar{b}b} = \frac{N_c\lambda_{HS}^2\sqrt{s}m_b^2(s-4m_b^2)^{3/2}}{4\pi(s-m_{h^0}^2)^2(s-m_{H^0}^2)^2}. \quad (16)$$

Indeed, the cross section does not vanish in the nonrelativistic limit of $s \to 4m_\eta^2$, provided that the process is kinematically allowed, $m_\eta > m_b$. Figure 4 shows the constraints from Fermi-LAT dwarf galaxy observations applicable to the model, translated as an upper limit for the portal coupling, λ_{HS}, as a function of the DM mass. Superimposed is the line where the observed relic abundance is produced by freeze-out. The dark blue shaded region is ruled out by the Fermi-LAT data [26], and the light blue shaded region is the expected exclusion region with 10 years of data, adapted from Ref. [32].

To produce the exclusion regions, we compare the annihilation cross section $v\sigma(\eta\eta \to b\bar{b})$ with the reported exclusion limit, for $m_\eta < m_W$. For $m_\eta > m_W$ the dominant annihilation channel is WW, for which the constraints are not available in the Fermi-LAT report. Based on model-independent analyses presented in Refs. [33,34], we estimate the constraint for this channel to be $v\sigma(\eta\eta \to WW) \approx 1.5v\sigma(\eta\eta \to b\bar{b})$ in our mass range of interest. That is, we compare the model prediction for the annihilation cross section in the WW channel to the reported upper limit for the $b\bar{b}$ cross section, scaled by a factor of 1.5, for a given value of the DM mass. As the DM mass increases further and the ZZ and h^0h^0 channels become kinematically allowed, we also include the annihilation cross section into these channels. For the purpose of simplicity and transparency of the analysis, we use the same rescaling factor for these channels as well; i.e., we compare the sum of the cross sections $\eta\eta \to WW$, ZZ, h^0h^0, to the $\bar{b}b$ limit rescaled by a factor of 1.5. This method will slightly overestimate the constraint from the ZZ-final state, but will not change the results qualitatively. Furthermore, the ZZ-final state is subleading, so quantitatively the effect is also relatively small.

This procedure results in kinks in the exclusion curve at $m_\eta = m_W, m_Z, m_{h^0}$. The kinks are nonphysical and would be removed by including the contribution from the off-shell processes $\eta\eta \to WW^*$, $ZZ^* \to 4f$, etc., where f is a SM fermion. To give a clearer comparison between this limit and

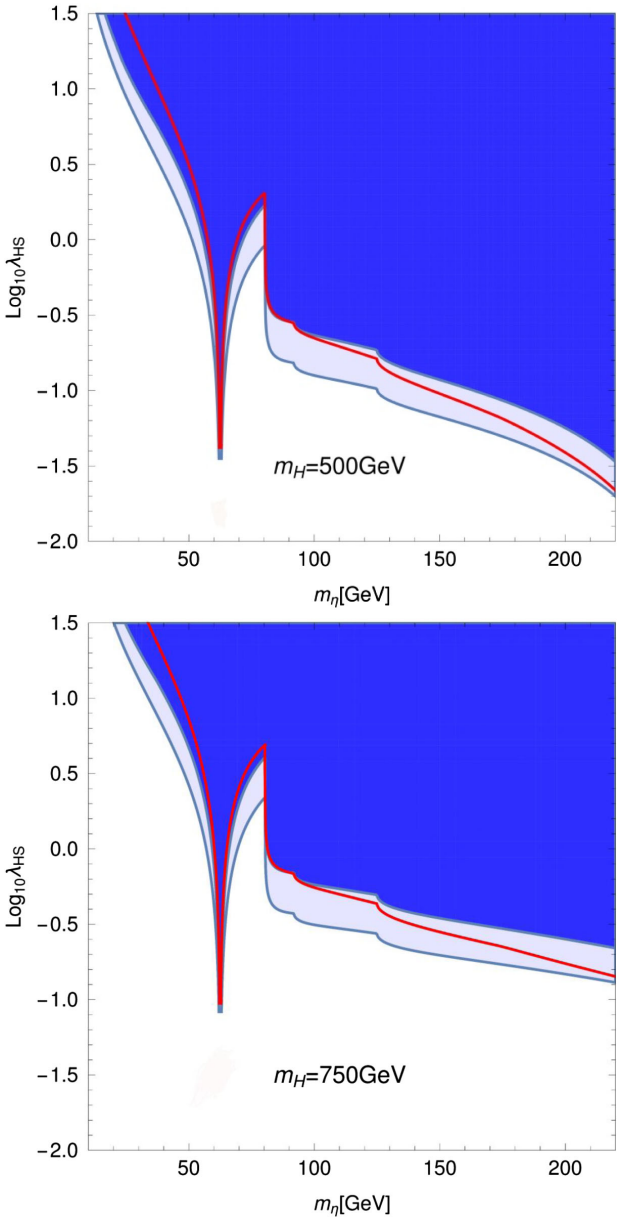

FIG. 4. Top panel: the indirect-detection constraints for $m_{H^0} = 500$ GeV. Bottom panel: same as the left panel, but for $m_{H^0} = 750$ GeV. In both panels the dark blue region is ruled out by the Fermi-LAT data and the light blue region is the expected exclusion region with 10 years of data. The red curve shows where the observed DM abundance is obtained.

the thermal annihilation cross section, shown by the red line, here we also remove the full-Higgs-width correction from the relic-abundance computation. The smoothing around the kinematic thresholds is expected to be similar for both the exclusion region and the relic-abundance line. A more detailed analysis of interpreting the Fermi-LAT constraints in terms of various final states is beyond the scope of this work.

We conclude that with the treatment described above, the thermal-relic cross section appears already excluded by the Fermi-LAT data for $m_\eta < m_W$ and will be probed up to $m_\eta \sim 250$ GeV with future data. However, to make conclusive statements of the fate of the model in light of indirect-detection constraints, a detailed analysis of the full set of annihilation final states is required.

IV. CONCLUSIONS

In this paper, we have considered a model framework that allows a paradigmatic thermal-relic WIMP to escape current direct-search limits and remain out of reach also for future experiments. The effect arises due to momentum-dependent interactions between the DM and ordinary matter, and it appears naturally in scenarios where the DM candidate is a pseudo-Goldstone boson of an approximate global symmetry [11,14,17,19].

We first outlined the general formulation of this type of models and then, to illustrate the effect more explicitly, considered how various observational constraints are implemented in the case where the hidden sector consists of a complex singlet scalar with an O(2) global symmetry. We demonstrated that in this model one can obtain the correct DM relic density and simultaneously remain out of the reach of current direct-search experiments.

In the tree-level analysis, the key feature is the momentum dependence of the DM interactions. However, since the global symmetry is only approximate, the effects of symmetry breaking must be addressed [12]. Generic and concrete origins of the slight violation of such symmetry are interactions with high-energy d.o.f. that are integrated out above the energy scales of the effective theory for the DM and the SM. We analyzed how the symmetry-breaking operators increase the direct-detection cross section. We found that even when symmetry breaking is present, the direct detection of such pseudo-Goldstone DM requires the future experiments to disentangle the signals of DM scattering from those of the neutrino background.

As our main result, we established how this type of DM can be observed by indirect detection. The annihilation cross section of the Goldstone boson DM is not suppressed by the incoming three-momentum, and therefore the constraints are similar to a vanilla WIMP candidate. We conclude that the future Fermi-LAT observations will be able to discover or exclude this type of DM with masses up to a few hundred GeV.

We showed the results for a simple extension of the SM, where a Goldstone DM consists of a single scalar field. Our results can be directly applied also to the case of a non-abelian symmetry where the Goldstone DM arises as a degenerate multiplet of dark pions [16,17]: On the one hand, the direct detection will become more efficient as the event rate will increase proportionally to the DM d.o.f. On the other hand, the indirect-detection constraint is independent of the DM multiplicity, and the conclusions from the constraints we have presented hold for any Goldstone DM within the class of models we considered in Sec. II.

A further interesting extension to study would be a scenario where the SM scalar sector is enlarged so that both DM and the Higgs boson arise as pseudo-Goldstone particles [8,15]. In this type of models, the interactions between the DM and ordinary matter would be further suppressed, and the origin of visible and dark matter would become more tightly tied together.

Finally, it would be interesting to study these models at finite temperature. This would lead to the determination of the consequences of such frameworks for the electroweak phase transition and associated possibilities for electroweak baryogenesis. A possible first-order phase transition in the hidden sector would also lead to generation of gravitational wave signals [35] possibly detectable with future detectors [36]. Complementary to the cosmological probes, collider signatures of such frameworks have been studied in [9,37], which in general are similar to those of a singlet extension of the SM.

ACKNOWLEDGMENTS

This work has been financially supported by the Academy of Finland Project No. 310130. V. K. acknowledges the H2020-MSCA-RISE-2014 Grant No. 645722 (NonMinimalHiggs) and the National Science Centre, Poland, the HARMONIA project under Contract No. UMO-2015/18/M/ST2/00518 and the discussion that followed the HARMONIA meeting. N. K. acknowledges financial support from the Väisälä foundation.

APPENDIX A: CROSS SECTIONS

Here we give the formulas for the computation of the annihilation cross section for the model considered in Sec. III. To make the equations more concise, it is useful to define the couplings

$$\begin{aligned}
\lambda_{\eta\eta h^0 h^0} &= (\lambda_{HS}+\lambda_X)c_\alpha^2 + 2\lambda_S s_\alpha^2,\\
\lambda_{\eta\eta H^0 H^0} &= (\lambda_{HS}+\lambda_X)s_\alpha^2 + 2\lambda_S c_\alpha^2,\\
\lambda_{\eta\eta h^0} &= (\lambda_{HS}+\lambda_X)vc_\alpha - 2\lambda_S w s_\alpha,\\
\lambda_{\eta\eta H^0} &= (\lambda_{HS}+\lambda_X)vs_\alpha + 2\lambda_S w c_\alpha,\\
\lambda_{h^0h^0h^0} &= 6\lambda_H v c_\alpha^3 + 3(\lambda_{HS}-\lambda_X)vs_\alpha^2 c_\alpha\\
&\quad -3(\lambda_{HS}-\lambda_X)ws_\alpha c_\alpha^2 - 6\lambda_S w s_\alpha^3,\\
\lambda_{h^0h^0H^0} &= \frac{1}{4}[(6\lambda_H+\lambda_{HS}-\lambda_X)vs_\alpha + (6\lambda_S+\lambda_{HS}-\lambda_X)wc_\alpha\\
&\quad +3(2\lambda_H-\lambda_{HS}+\lambda_X)vs_{3\alpha} + 3(\lambda_{HS}-2\lambda_S-\lambda_X)wc_{3\alpha}],\\
\lambda_{h^0H^0H^0} &= \frac{1}{4}[(6\lambda_H+\lambda_{HS}-\lambda_X)vc_\alpha - (6\lambda_S+\lambda_{HS}-\lambda_X)ws_\alpha\\
&\quad -3(2\lambda_H-\lambda_{HS}+\lambda_X)vc_{3\alpha} + 3(\lambda_{HS}-2\lambda_S-\lambda_X)ws_{3\alpha}],\\
\lambda_{H^0H^0H^0} &= 6\lambda_H v s_\alpha^3 + 3(\lambda_{HS}-\lambda_X)vs_\alpha c_\alpha^2 + 3(\lambda_{HS}-\lambda_X)ws_\alpha^2 c_\alpha\\
&\quad +6\lambda_S w c_\alpha^3,
\end{aligned} \tag{A1}$$

and

$$\begin{aligned}
y_{h^0} &= \frac{m_f}{v}c_\alpha, \qquad y_{H^0} = \frac{m_f}{v}s_\alpha,\\
g_{h^0Z} &= \frac{v(g^2+g'^2)}{2}c_\alpha, \qquad g_{h^0W} = \frac{vg^2}{2}c_\alpha,\\
g_{H^0Z} &= \frac{v(g^2+g'^2)}{2}s_\alpha, \qquad g_{H^0W} = \frac{vg^2}{2}s_\alpha,
\end{aligned} \tag{A2}$$

where we have used the shorthand notations $s_x \equiv \sin x$ and $c_x \equiv \cos x$. The annihilation cross section to fermion final states is

$$\begin{aligned}
\sigma_{\eta\eta\to\bar{f}f} &= \frac{N_c m_f^2 \beta_f^3}{8\pi\beta_\eta (s-m_{h^0}^2)^2(s-m_{H^0}^2)^2}\\
&\quad \times [(\lambda_{HS}+\lambda_X)s - 2\lambda_X(s_\alpha^2 m_{h^0}^2 + c_\alpha^2 m_{H^0}^2)]^2,
\end{aligned} \tag{A3}$$

where

$$\beta_x \equiv \sqrt{1-\frac{4m_x^2}{s}}. \tag{A4}$$

The annihilation cross section to electroweak vector boson final states is

$$\begin{aligned}
\sigma_{\eta\eta\to VV} &= \frac{\delta_V \beta_V (12m_V^4 - 4m_V^2 s + s^2)}{16\pi s\beta_\eta (s-m_{h^0}^2)^2(s-m_{H^0}^2)^2}\\
&\quad \times [(\lambda_{HS}+\lambda_X)s - 2\lambda_X(s_\alpha^2 m_{h^0}^2 + c_\alpha^2 m_{H^0}^2)]^2,
\end{aligned} \tag{A5}$$

where $\delta_V = 1,\ 1/2$ for $W^\pm$ and Z boson final states, respectively.

Finally, the cross sections for annihilation into the h^0h^0 final state is

$$\begin{aligned}
\sigma_{\eta\eta\to h^0h^0} &= \frac{\beta_{h^0}}{32\pi s\beta_\eta}\left[\frac{16\lambda_{\eta\eta h^0}^4}{(s-2m_{h^0}^2)^2}\right.\\
&\quad + \left(\lambda_{\eta\eta h^0 h^0} + \frac{\lambda_{h^0h^0h^0}\lambda_{\eta\eta h^0}}{s-m_{h^0}^2} + \frac{\lambda_{h^0h^0H^0}\lambda_{\eta\eta H^0}}{s-m_{H^0}^2}\right)^2\\
&\quad \left. - \frac{8\lambda_{\eta\eta h^0}^2}{s-2m_{h^0}^2}\left(\lambda_{\eta\eta h^0 h^0} + \frac{\lambda_{h^0h^0h^0}\lambda_{\eta\eta h^0}}{s-m_{h^0}^2} + \frac{\lambda_{h^0h^0H^0}\lambda_{\eta\eta H^0}}{s-m_{H^0}^2}\right)\right].
\end{aligned} \tag{A6}$$

In our scenario, the pseudo-Goldstone boson, η, is lighter than the scalar H^0, and we do not consider final states h^0H^0 and H^0H^0. However, in a general setup, the cross section for the H^0H^0 final state can be obtained from Eq. (A6) by exchanging $h^0 \leftrightarrow H^0$. The cross section for the mixed final state h^0H^0 is lengthy and not particularly illuminating, and we do not report that explicitly here.

APPENDIX B: THE NONLINEAR REPRESENTATION TREATMENT

In the nonlinear representation, our starting point is the Lagrangian

$$\mathcal{L} = \frac{1}{2}\mathrm{Tr}[\partial_\mu S^\dagger \partial^\mu S] - V(H,S), \tag{B1}$$

where

$$H = \begin{pmatrix} \pi^+ \\ \frac{1}{\sqrt{2}}(v+\phi+i\pi^0) \end{pmatrix}, \quad S = \frac{w+\sigma}{\sqrt{N}} e^{i\eta^a X^a/w}, \tag{B2}$$

and X^a, $a = 1,\ldots,N$, are the broken generators. The scalar potential is given by

$$\begin{aligned} V(H,S) = {} & \mu_H^2 H^\dagger H + \frac{1}{2}\mu_S^2 \mathrm{Tr}[S^\dagger S] + \lambda_H (H^\dagger H)^2 \\ & + \frac{\lambda_{HS}}{2}(H^\dagger H)\mathrm{Tr}[S^\dagger S] + \frac{\lambda_S}{4}\mathrm{Tr}[S^\dagger S]^2 \\ & - \frac{1}{4}\mu_X^2(\mathrm{Tr}[S^2] + \mathrm{Tr}[S^{\dagger 2}]), \end{aligned} \tag{B3}$$

where we have for simplicity set the quartic symmetry-breaking coupling, λ_X, to zero.

The minimization conditions are as in Eq. (6) for $\lambda_X = 0$,

$$\begin{aligned} \mu_H^2 &= -\lambda_H v^2 - \frac{1}{2}\lambda_{HS} w^2, \\ \mu_S^2 &= -\lambda_S w^2 - \frac{1}{2}\lambda_{HS} v^2 + \mu_X^2, \end{aligned} \tag{B4}$$

and we again define the mass eigenstates via a rotation

$$\begin{pmatrix} h^0 \\ H^0 \end{pmatrix} = \begin{pmatrix} \cos\alpha & -\sin\alpha \\ \sin\alpha & \cos\alpha \end{pmatrix} \begin{pmatrix} \phi \\ \sigma \end{pmatrix}, \tag{B5}$$

with the mixing angle defined as

$$\tan(2\alpha) = \frac{-\lambda_{HS} v w}{\lambda_H v^2 - \lambda_S w^2}. \tag{B6}$$

The parameters λ_H, λ_S, λ_{HS}, and μ_X^2 can then be rewritten in terms of the masses of the scalars and their mixing angle,

$$\begin{aligned} \lambda_H &= \frac{1}{4v^2}[(m_{H^0}^2 + m_{h^0}^2) - (m_{H^0}^2 - m_{h^0}^2)\cos(2\alpha)], \\ \lambda_S &= \frac{1}{4w^2}[(m_{H^0}^2 + m_{h^0}^2) + (m_{H^0}^2 - m_{h^0}^2)\cos(2\alpha)], \\ \lambda_{HS} &= \frac{\sin(2\alpha)}{2vw}(m_{H^0}^2 - m_{h^0}^2), \\ \mu_X^2 &= \frac{1}{2}m_\eta^2. \end{aligned} \tag{B7}$$

In the following, we will compute the effective couplings entering the direct- and indirect-detection cross sections to be compared with the linear-representation results, Sec. III and Appendix A. For simplicity, we will fix $N = 1$. The relevant terms of the Lagrangian for direct and indirect detection and relic density calculations are

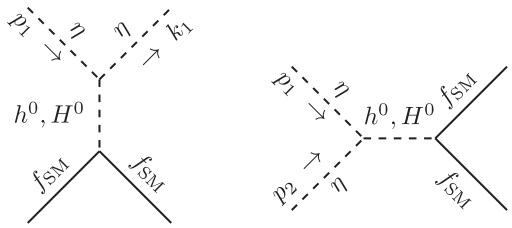

FIG. 5. Relevant diagrams for direct and indirect detection.

$$\begin{aligned} V_{\mathrm{int}} \supset {} & -\frac{m_\eta^2}{w}[\sin\alpha h^0 - \cos\alpha H^0]\eta^2 \\ & + \frac{1}{w}[\sin\alpha h^0 - \cos\alpha H^0](\partial_\mu \eta)^2, \end{aligned} \tag{B8}$$

with the corresponding diagrams shown in Fig. 5. For indirect detection we show here only the fermionic final states for simplicity.

In the direct-detection process, λ_{eff} corresponding to that of Eqs. (13) and (14) has the form

$$\begin{aligned} \lambda_{\mathrm{eff}}^{\mathrm{NL}} &= \frac{\sin(2\alpha)(m_{h^0}^2 - m_{H^0}^2)}{vw(m_{h^0}^2 - t)(m_{H^0}^2 - t)}(-m_\eta^2 - (-p_1\cdot k_1)) \\ &= \frac{\sin(2\alpha)(m_{h^0}^2 - m_{H^0}^2)}{vw(m_{h^0}^2 - t)(m_{H^0}^2 - t)}\left(-m_\eta^2 - \frac{1}{2}(t - 2m_\eta^2)\right) \\ &= \frac{\sin(2\alpha)(m_{h^0}^2 - m_{H^0}^2)}{vw(m_{h^0}^2 - t)(m_{H^0}^2 - t)}\cdot\frac{-t}{2}. \end{aligned} \tag{B9}$$

Writing $\lambda_{\mathrm{eff}}^{\mathrm{NL}}$ in terms of λ_{HS} using Eq. (B7), we obtain the same expression (up to an overall sign) as in the linear case, Eq. (14).

In the indirect detection, on the other hand, the corresponding effective coupling is given by

$$\begin{aligned} \lambda_{\mathrm{eff,ID}}^{\mathrm{NL}} &= \frac{\sin(2\alpha)(m_{h^0}^2 - m_{H^0}^2)}{vw(m_{h^0}^2 - s)(m_{H^0}^2 - s)}(-m_\eta^2 - (p_1\cdot p_2)) \\ &= \frac{\sin(2\alpha)(m_{h^0}^2 - m_{H^0}^2)}{vw(m_{h^0}^2 - s)(m_{H^0}^2 - s)}\left(-m_\eta^2 - \frac{1}{2}(s - 2m_\eta^2)\right) \\ &= \frac{\sin(2\alpha)(m_{h^0}^2 - m_{H^0}^2)}{vw(m_{h^0}^2 - s)(m_{H^0}^2 - s)}\cdot\frac{-s}{2}. \end{aligned} \tag{B10}$$

Again, writing $\lambda_{\mathrm{eff,ID}}^{\mathrm{NL}}$ in terms of λ_{HS} using Eq. (B7), we recover the same cross sections as in the linear case in the limit $\lambda_X = 0$; see, e.g., the cross section to fermionic final states, Eq. (A3).

[1] D. S. Akerib *et al.* (LUX Collaboration), Phys. Rev. Lett. **118**, 251302 (2017).
[2] X. Cui *et al.* (PandaX-II Collaboration), Phys. Rev. Lett. **119**, 181302 (2017).
[3] E. Aprile *et al.* (XENON Collaboration), Phys. Rev. Lett. **121**, 111302 (2018).
[4] J. McDonald, Phys. Rev. Lett. **88**, 091304 (2002).
[5] L. J. Hall, K. Jedamzik, J. March-Russell, and S. M. West, J. High Energy Phys. 03 (2010) 080.
[6] N. Bernal, M. Heikinheimo, T. Tenkanen, K. Tuominen, and V. Vaskonen, Int. J. Mod. Phys. A **32**, 1730023 (2017).
[7] M. Pospelov, A. Ritz, and M. B. Voloshin, Phys. Lett. B **662**, 53 (2008).
[8] T. Alanne, H. Gertov, F. Sannino, and K. Tuominen, Phys. Rev. D **91**, 095021 (2015).
[9] D. Barducci, A. Bharucha, N. Desai, M. Frigerio, B. Fuks, A. Goudelis, S. Kulkarni, G. Polesello, and D. Sengupta, J. High Energy Phys. 01 (2017) 078.
[10] C. Gross, O. Lebedev, and T. Toma, Phys. Rev. Lett. **119**, 191801 (2017).
[11] D. Azevedo, M. Duch, B. Grzadkowski, D. Huang, M. Iglicki, and R. Santos, Phys. Rev. D **99**, 015017 (2019).
[12] D. Azevedo, M. Duch, B. Grzadkowski, D. Huang, M. Iglicki, and R. Santos, J. High Energy Phys. 01 (2019) 138.
[13] K. Ishiwata and T. Toma, J. High Energy Phys. 12 (2018) 089.
[14] R. Balkin, M. Ruhdorfer, E. Salvioni, and A. Weiler, J. Cosmol. Astropart. Phys. 11 (2018) 050.
[15] T. Alanne, D. Buarque Franzosi, M. T. Frandsen, and M. Rosenlyst, J. High Energy Phys. 12 (2018) 088.
[16] T. Hur, D.-W. Jung, P. Ko, and J. Y. Lee, Phys. Lett. B **696**, 262 (2011).
[17] T. Hur and P. Ko, Phys. Rev. Lett. **106**, 141802 (2011).
[18] S. Bhattacharya, B. Melić, and J. Wudka, J. High Energy Phys. 02 (2014) 115.
[19] M. Heikinheimo, A. Racioppi, M. Raidal, C. Spethmann, and K. Tuominen, Mod. Phys. Lett. A **29**, 1450077 (2014).
[20] A. Ilnicka, T. Robens, and T. Stefaniak, Mod. Phys. Lett. A **33**, 1830007 (2018).
[21] G. Aad *et al.* (ATLAS Collaboration), J. High Energy Phys. 11 (2015) 206.
[22] V. Khachatryan *et al.* (CMS Collaboration), J. High Energy Phys. 02 (2017) 135.
[23] J. M. Alarcon, J. Martin Camalich, and J. A. Oller, Phys. Rev. D **85**, 051503 (2012).
[24] J. M. Alarcon, L. S. Geng, J. Martin Camalich, and J. A. Oller, Phys. Lett. B **730**, 342 (2014).
[25] J. M. Cline, K. Kainulainen, P. Scott, and C. Weniger, Phys. Rev. D **88**, 055025 (2013); **92**, 039906(E) (2015).
[26] A. Albert *et al.* (DES and Fermi-LAT Collaborations), Astrophys. J. **834**, 110 (2017).
[27] V. Barger, P. Langacker, M. McCaskey, M. Ramsey-Musolf, and G. Shaughnessy, Phys. Rev. D **79**, 015018 (2009).
[28] J. M. Cline and K. Kainulainen, J. Cosmol. Astropart. Phys. 01 (2013) 012.
[29] D. de Florian *et al.* (LHC Higgs Cross Section Working Group), *Handbook of LHC Higgs Cross Sections: 4. Deciphering the Nature of the Higgs Sector* (CERN, Geneva, 2017).
[30] S. Dittmaier *et al.* (LHC Higgs Cross Section Working Group), *Handbook of LHC Higgs Cross Sections: 1. Inclusive Observables* (CERN, Geneva, 2011).
[31] J. Billard, L. Strigari, and E. Figueroa-Feliciano, Phys. Rev. D **89**, 023524 (2014).
[32] E. Charles *et al.* (Fermi-LAT Collaboration), Phys. Rep. **636**, 1 (2016).
[33] K. Boddy, J. Kumar, D. Marfatia, and P. Sandick, Phys. Rev. D **97**, 095031 (2018).
[34] S. J. Clark, B. Dutta, and L. E. Strigari, Phys. Rev. D **97**, 023003 (2018).
[35] P. Schwaller, Phys. Rev. Lett. **115**, 181101 (2015).
[36] K. Kannike and M. Raidal, arXiv:1901.03333.
[37] K. Huitu, N. Koivunen, O. Lebedev, S. Mondal, and T. Toma, arXiv:1812.05952.